First published online as a Review in Advance on November 21, 2007

Extending X-Ray Crystallography to Allow the Imaging of Noncrystalline Materials, Cells, and Single Protein Complexes

Jianwei Miao,[1] Tetsuya Ishikawa,[2] Qun Shen,[3] and Thomas Earnest[4]

[1]Department of Physics and Astronomy, University of California, Los Angeles, California 90095; email: miao@physics.ucla.edu; [2]RIKEN SPring-8 Center, Kouto, Sayo, Hyogo 679-5148, Japan; [3]Advanced Photon Source, Argonne National Laboratory, Argonne, Illinois 60439; [4]Physical Biosciences Division, Lawrence Berkeley National Laboratory, Berkeley, California 94720

Annu. Rev. Phys. Chem. 2008. 59:387–410

The *Annual Review of Physical Chemistry* is online at http://physchem.annualreviews.org

This article's doi: 10.1146/annurev.physchem.59.032607.093642

0066-426X/08/0505-0387$20.00

Key Words

X-ray diffraction microscopy, oversampling method, lensless imaging, phase retrieval, noncrystalline specimen, single-molecule imaging, X-ray free electron lasers

Abstract

In 1999, researchers extended X-ray crystallography to allow the imaging of noncrystalline specimens by measuring the X-ray diffraction pattern of a noncrystalline specimen and then directly phasing it using the oversampling method with iterative algorithms. Since then, the field has evolved moving in three important directions. The first is the 3D structural determination of noncrystalline materials, which includes the localization of the defects and strain field inside nanocrystals, and quantitative 3D imaging of disordered materials such as nanoparticles and biomaterials. The second is the 3D imaging of frozen-hydrated whole cells at a resolution of 10 nm or better. A main thrust is to localize specific multiprotein complexes inside cells. The third is the potential of imaging single large protein complexes using extremely intense and ultrashort X-ray pulses. In this article, we review the principles of this methodology, summarize recent developments in each of the three directions, and illustrate a few examples.

INTRODUCTION

Von Laue's discovery of X-ray diffraction from crystals nearly 100 years ago marked the beginning of a new era for visualizing 3D atomic structures inside crystals. Indeed, X-ray crystallography has since made a tremendous impact in physics, chemistry, materials sciences, biology, and other areas. It has now reached a point at which it can determine almost any structure, as long as good-quality crystals are obtained. Many samples, however, cannot be accessed by this approach, such as amorphous and disordered materials including glasses, polymers, strains and defects in crystals, quantum dots and wires, dislocation and deformation structures, and some inorganic nanostructures. In biology, structures such as whole cells, organelles, viruses, and many important protein molecules cannot or are difficult to crystallize; hence their structures are not accessible by X-ray crystallography. Overcoming these limitations requires the employment of different techniques and methods, such as nuclear magnetic resonance spectroscopy (1) and cryo-electron microscopy (2, 3). One promising approach currently under rapid development is extending the methodology of X-ray crystallography to allow the structural determination of noncrystalline specimens, which we call X-ray diffraction microscopy (or lensless imaging) (4, 5). **Figure 1** shows the principles of X-ray diffraction microscopy. When a coherent wave of X rays illuminates a noncrystalline specimen, the far-field diffraction intensities are continuous and weak. The continuous intensities can be sampled at an arbitrary frequency (6). When the sample frequency is sufficiently finer than the Nyquist interval (i.e., the inverse of the sample size) so that the number of independent intensity points is more than the number of unknown variables, the phases are encoded in the intensities (7) and can be retrieved directly using an iterative algorithm (8–11). Here the number of unknown variables represents the voxel number of an array sampling the sample structure.

Historically, Sayre (12, 13) first suggested the idea of X-ray diffraction microscopy. It was not until in 1999 that Miao et al. (14) carried out the first experimental

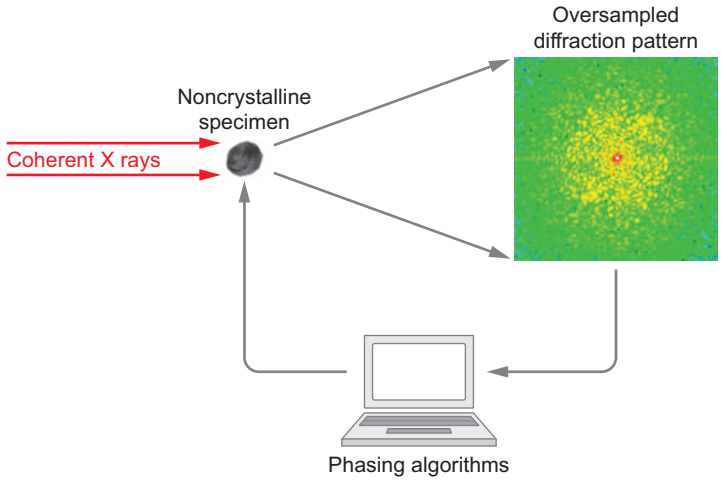

Figure 1
The principles of X-ray diffraction microscopy.

demonstration. Since then, over 20 groups worldwide have applied the technique successfully to imaging a variety of samples, ranging from nanoparticles, nanocrystals, and biomaterials to whole cells (15–39). A biennial international workshop series has been organized to discuss current progress and the future potential of this emerging field (40). In this article, we review the principles of the oversampling method with iterative algorithms and illustrate a few applications of X-ray diffraction microscopy to imaging noncrystalline materials and biological cells. Finally, we discuss the potential of imaging single large protein complexes using extremely intense and ultrafast X-ray free electron laser (XFEL) pulses.

XFEL: X-ray free electron laser

THE OVERSAMPLING METHOD AND ITERATIVE ALGORITHMS

The Phase Problem

A typical X-ray diffraction experiment involves measuring a series of far-field diffraction patterns from the specimen and inverting the diffraction patterns to reconstruct the specimen structure. In principle, the intensity of each diffraction pattern depends on the exact arrangement of atom positions in the specimen, and by quantitatively analyzing all intensities, one can retrieve the exact locations of all atoms in the structure. Unfortunately, this is not as easy as one would think because the measured intensity pattern is only directly related to the modulus of a Fourier transform of the specimen's electron density, and the phase information is not easily available. To reconstruct the electron density, one needs both the magnitudes and the phases, as in any inverse Fourier transform for reconstruction. This loss of phase information is the fundamental phase problem in diffraction measurements and can be classified into a greater category of inversion problems that exist in all wave-field propagation measurements in optics and other related fields (41, 42).

Ever since the discovery of X-ray diffraction from crystals in the early twentieth century, efforts to seek solutions to the phase problem have been central to work in X-ray crystallography. Scientists solved early small-molecule structures by using the fact that the measured intensity is a direct Fourier transform of the density autocorrelation function—the so-called Patterson function in crystallography (43). By looking at all possible interatomic vector arrangements in trial structures, one can find the structure that best fits the experimentally measured Patterson. As the structures get larger and more complex, however, this simple trial-and-error method becomes more difficult owing to the exponential growth in the number of interatomic vectors in three dimensions. Over the years many more powerful phasing methods have been developed, including direct methods (44), isomorphous replacements (45), molecular replacement (46), multiple anomalous dispersion (47, 48), and solvent flattening (49). The use of other experimental measured phase information, such as noncrystallographic symmetry (50, 51), molecular envelope (52) or triplet phases (53, 54), can also be exploited to solve protein crystal structures and is of current research interest.

The Oversampling Method

When the specimen is noncrystalline, the diffraction pattern becomes continuous and weak, in contrast to the sharp Bragg peaks from a crystal. One can solve the phase problem of the continuous diffraction pattern using a different class of phasing techniques called the oversampling method. According to Shannon's (55) sampling theorem, when a function is band limited within (0, a), its Fourier transform sampled at the Nyquist interval ($1/a$) fully and exactly determines the function itself (**Figure 2*a***). When comparing Shannon's sampling with X-ray diffraction from crystals (**Figure 2*b***), we can see that the sampling frequency is the same (13). Theoretically, an infinite number of electron density functions can produce the same modulus of the Fourier transform sampled at the Nyquist interval, which is defined as indistinguishable (**Figure 2*c***) (6, 9). Based on the argument that the autocorrelation function of any object is twice the size of the object itself, Bates (56) concluded in 1982 that if and only if a diffraction pattern is sampled at a frequency twice finer than the Nyquist interval, phases can be uniquely retrieved from the intensity. In 1998, Miao et al. (7) showed that Bates's conclusion is overly restrictive and proposed a different explanation. They introduced the oversampling ratio (σ) to characterize the degree of oversampling, where $\sigma = \sigma_x\sigma_y\sigma_z$ and σ_x, σ_y, and σ_z represent the sampling frequency divided by the Nyquist interval in the x, y, and z axis, respectively. When $\sigma > 2$, the number of correlated intensity points is more than the number of unknown variables, and the modulus of the Fourier transform can in principle uniquely determine the electron density (7), which is defined as distinguishable (**Figure 2*d***). Oversampling a diffraction pattern requires good coherence of the incident waves. The higher the oversampling degree is, the better the required coherence. It is the coherence that causes the correlation of the diffraction intensity and provides the phase information (16). We note that oversampling a diffraction pattern is different from a support constraint. When the diffraction pattern is sampled at a frequency finer than the Nyquist interval but not sufficiently finer, there is a support, but phases are not unique. The unique phases exist only when the sampling frequency is sufficiently finer than the Nyquist interval (i.e., $\sigma > 2$).

Iterative Algorithms

Oversampling a diffraction pattern with $\sigma > 2$ encodes the phases in the diffraction intensity. It is, however, a daunting task to find the unique phases from the number of correlated intensity points (i.e., nonlinear equations). An efficient approach uses global optimization methods such as error reduction (8), hybrid input-output (8), difference map (10), shrink-wrap (11), and Hamiltonian methods (57), all of which are iterated back and forth between real and reciprocal space (58). One approach that shows good convergence and reliable phase retrieval is called the guided hybrid input-output algorithm (35, 38, 59) as illustrated below:

1. The approach starts typically with 16 independent reconstructions on an oversampled X-ray diffraction pattern, in which different random phases are used as initial inputs.

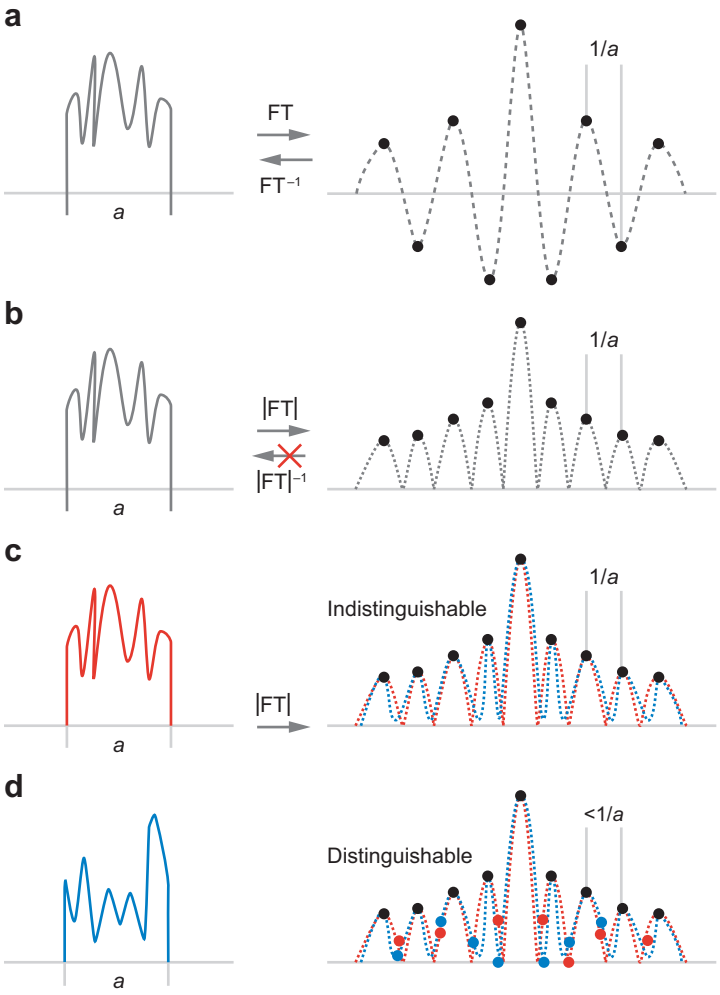

Figure 2

(*a*) A band-limited function and its Fourier transform (FT) sampled at the Nyquist interval (*black dots*). (*b*) The electron density of a unit cell inside a crystal and its modulus of the FT sampled at Bragg peak frequency at which the crystal lattice effect is ignored. (*c*) An infinite number of electron density functions can produce the same modulus of the FT sampled at the Nyquist interval (*black dots*). (*d*) If the modulus of the FT is sampled at a frequency finer than the Nyquist interval (i.e., $\sigma > 2$), the modulus of the Fourier transform (*the black and red dots versus the black and blue dots*) can in principle uniquely determine the electron density.

2. Each reconstruction is iterated back and forth between real and reciprocal space. For the initial 500 iterations, the electron density outside the support and the negative electron density inside the support are slowly pushed to zero. In reciprocal space, the Fourier modulus remains unchanged and only the phases are updated.

3. For the next 500 iterations, a procedure called boundary pushing is adopted, in which the electron density outside the support and the negative electron density inside the support are quickly pushed to zero. This step imposes a stronger constraint than step 2.
4. After 1000 iterations, 16 independently reconstructed images are obtained, defined as the zeroth generation. An R_F is calculated for each image,

$$R_F = \frac{\sum_{k_x, k_y} ||F_{exp}| - \alpha |F_{cal}||}{\sum_{k_x, k_y} |F_{exp}|}, \quad (1)$$

where $|F_{exp}|$ and $|F_{cal}|$ represent the experimental and calculated Fourier modulus, respectively; k_x and k_y are the coordinates in reciprocal space; and α is the scaling factor.
5. A seed image (ρ_{seed}) is chosen that corresponds to the smallest R_F. The other 15 images (ρ_{old}) are aligned to the seed using cross-correlation.
6. A set of new images (ρ^i_{new}) is calculated by

$$\rho^i_{new} = \sqrt{\rho_{seed} \times \rho^i_{old}} \quad i = 1, 2, \ldots, 16, \quad (2)$$

which is used as the initial input for the next generation. Equation 2 merges the best image in the current generation with each of the 16 images, so the favorable gene (i.e., the smallest R_F) is passed on to the succeeding generations. Furthermore, density fluctuations in the new image are significantly reduced after the multiplication of the two independent images.
7. Steps 1–6 are repeated, and, usually after the eighth generation, the final 16 images become consistent.

To show the good convergence and consistency of the guided hybrid input-output algorithm, we illustrate an example on phasing an oversampled X-ray diffraction pattern from a GaN quantum-dot particle (35). **Figure 3** shows the 16 reconstructed images at the zeroth and eighth generation. The smallest R_F at the zeroth and eighth generation is 14.9% and 8.25%, respectively. The 16 reconstructed images are virtually identical at the eighth generation, and the five images corresponding to the smallest R_F are averaged to be the final reconstructed image for the diffraction pattern.

3D STRUCTURAL DETERMINATION OF NONCRYSTALLINE MATERIALS

Because X-ray wavelengths are on the order of the size of atoms, and X rays have a longer penetration depth than electrons, scientists have long dreamed of atomic-resolution X-ray microscopes that could visualize the arrangement of atoms in three dimensions. X rays, however, are much more difficult to focus than electrons. By using X-ray optics, the smallest focal spot currently attainable is ~30 nm for hard X rays (60) and ~15 nm for soft X rays (61). Furthermore, when the focal spot of soft X rays reaches 15 nm, the depth of focus becomes less than 0.5 μm (62), which limits the thickness of the sample under investigation. By avoiding the use of lenses, X-ray diffraction microscopy overcomes the limitations imposed by X-ray optics and has

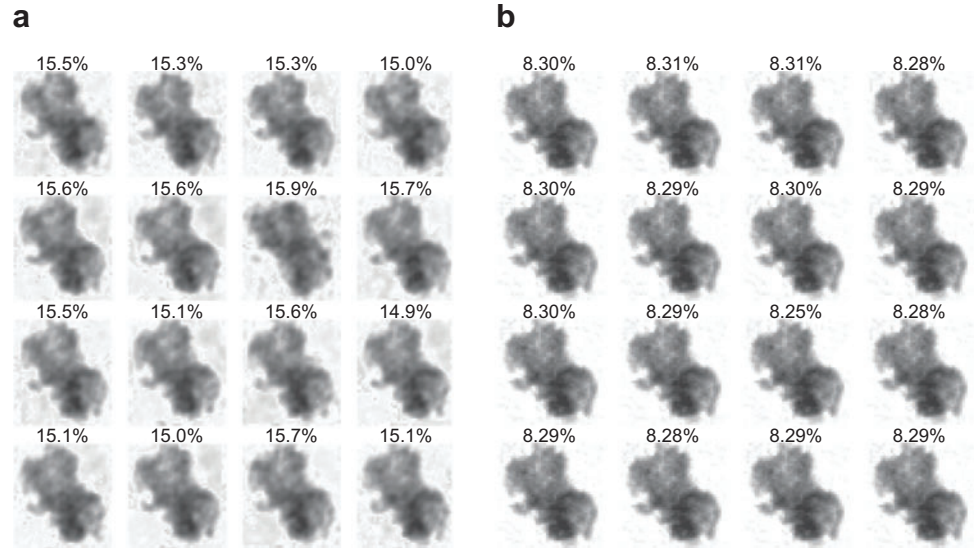

Figure 3

Phasing an oversampled X-ray diffraction pattern from a GaN quantum-dot particle by the guided hybrid input-output algorithm. The 16 reconstructed images at the (*a*) zeroth and (*b*) eighth generation, where the R_F value for each image is shown. Figure taken from Reference 35.

been successfully applied to the structural determination of noncrystalline materials such as nanoparticles, nanocrystals, and biological materials (15–39). Currently two versions of X-ray diffraction microscopy are under rapid development. The first is based on forward X-ray diffraction, and the reconstructed images represent the electron density of the sample structure (16, 19, 20, 22, 27, 28, 30, 33–39, 63). The second employs Bragg diffraction from the sample's crystal planes, which has been used not only to determine the shape of a nanocrystal, but also to map out the strain field inside the nanocrystal (5, 15, 23, 32).

To illustrate the unique capability of X-ray diffraction microscopy, we use the 3D structural determination of a GaN quantum-dot nanoparticle as an example (28, 35). The GaN quantum-dot particles were heat treated in a flowing stream of pure N_2 gas (flow rate of 100 ml min^{-1}) at 900°C for 24 h. The nitrogen atmosphere created an environment with a low partial pressure of oxygen, thus oxidizing the GaN particles at a controllable rate and forming a thin shell of Ga oxide on the GaN core (64). By using a third-generation synchrotron undulator with 5-keV X rays, investigators collected a set of 27 oversampled diffraction patterns from a single GaN quantum-dot nanoparticle with the tilt range of –69.4° to +69.4°. The 27 diffraction patterns were directly phased using the guided hybrid input-output algorithm and then inverted to a 3D image. **Figure 4** shows isosurface renderings of the reconstructed 3D image. A distinctive feature of the particle is the platelet-like structure. By examining the 3D surface morphology, one can observe the formation of small islands with varied size on the particle's surface, which results from the surface oxidation of GaN platelets

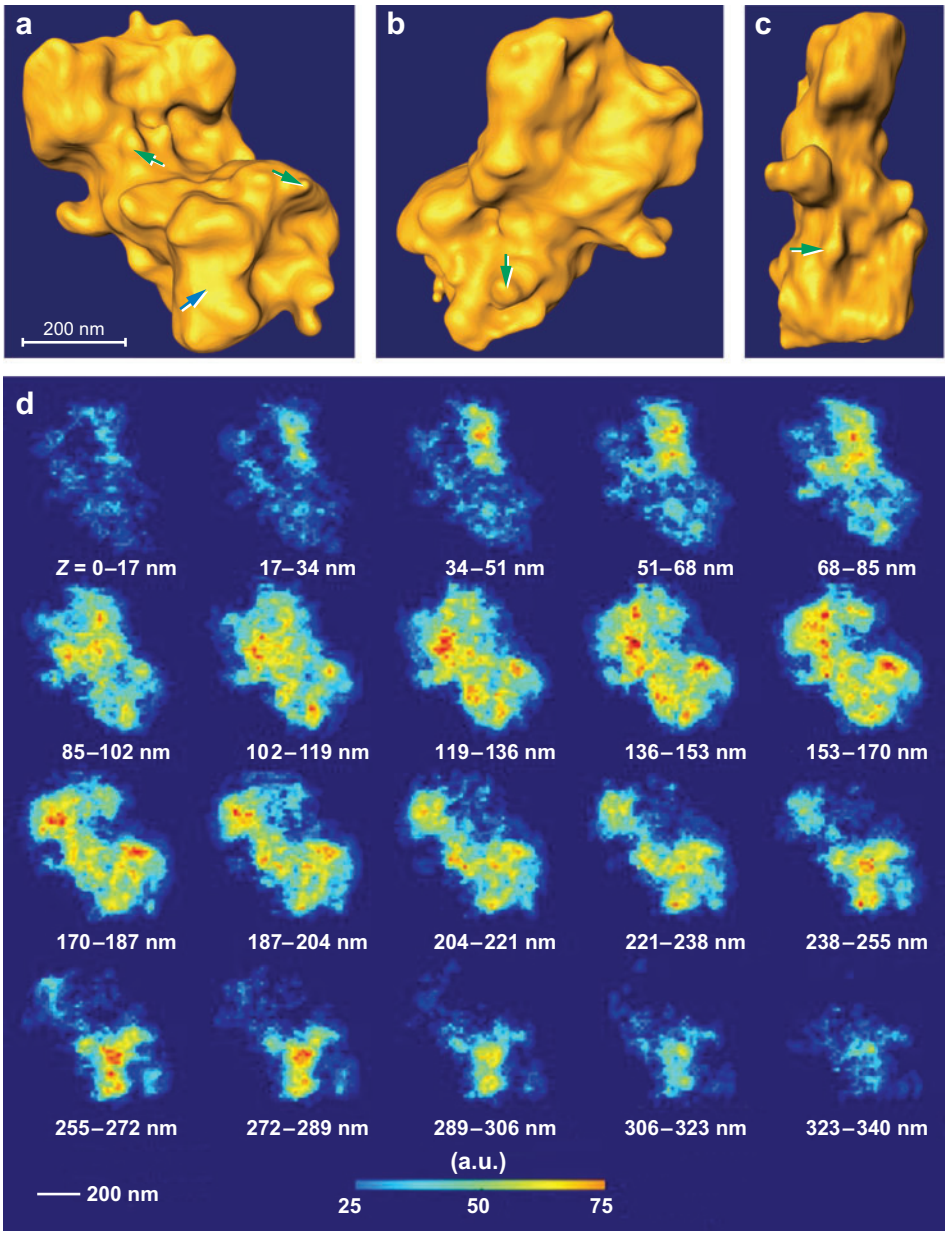

Figure 4

Isosurface rendering of a reconstructed 3D GaN quantum-dot particle, showing (*a*) the front, (*b*) back, and (*c*) side view. A platelet is indicated by a blue arrow in panel *a*. The formation of small islands (*green arrows*) on the surface of the particles is clearly visible. (*d*) The 3D internal structure of the GaN quantum-dot particle. The 3D GaN-Ga_2O_3 core shell structure is clearly visible, with the low electron density (*blue*) corresponding to β-Ga_2O_3 and the high electron density (*red*) corresponding to the GaN cores. Figure taken from Reference 35.

after the heat treatment. To quantitatively visualize the 3D internal structure, one computationally slices the particle slice by slice, with each corresponding to 17 nm (**Figure 4*d***). **Figure 4*d*** shows that the high-density region, concentrated near the center of the platelets, is surrounded by low density. The low electron density is from the β-Ga_2O_3 regions of the particle, whereas the high electron density is from the GaN particle. During the GaN surface-oxidation process, small island-like features of β-Ga_2O_3 formed on the surface of the platelets, which have a lower quality of crystallinity than the GaN cores and give rise to the low electron density. This observation provides direct evidence of the existence of a 3D GaN-Ga_2O_3 core shell structure in heat-treated GaN platelets.

X-ray diffraction microscopy has emerged as a powerful technique for the 3D imaging and characterization of a wide range of noncrystalline materials, including porous materials, semiconductors, quantum dots and wires, inorganic nanostructures, and biomaterials. Compared with transmission electron or scanning probe microscopy (65, 66), X-ray diffraction microscopy does not require destructive sample preparation and can quantitatively image thick materials in three dimensions. Although the highest resolution achieved to date is ∼7 nm (67), the ultimate resolution is only limited by the X-ray wavelengths. As more brilliant X-ray sources emerge, such as XFELs that are under rapid development worldwide (68, 69), it is anticipated that X-ray diffraction microscopy will eventually achieve near-atomic resolution in three dimensions.

STRUCTURE OF WHOLE CELLS

A full and comprehensive understanding of biological processes requires knowledge of the 3D structure of the cell's constituents at resolutions that range from atomic (as in the structure of proteins and nucleic acids) to the somewhat lower-resolution information about the localization, and changes in localization, of these molecules and the molecular assemblies they form (70). With the structural elucidation of the components by structural genomics (71) and other projects, it is necessary to develop resources and approaches to study these molecules' interactions and their dynamic localization in the cell. As informative as the atomic-resolution studies of proteins have proven to be, knowledge of the structure and dynamics of the cell's molecular interaction networks as well as their localization is critical. Recent studies of these protein-protein interaction networks indicate that within the cell most proteins exist and function as components of multiprotein complexes—some stable but many transient and weakly associated. Many of these complexes, and their associated functions, demonstrate tightly coupled spatial and temporal regulation in eukaryotic (72, 73) and prokaryotic cells (74, 75).

Although light microscopy can routinely study dynamic processes in living cells (76), its resolution is currently limited to ∼200 nm. In some special cases, better resolutions (up to 20 nm) may be obtained using techniques such as stimulated emission depletion microscopy (77) or photoactivated localization microscopy (78). To achieve considerably higher resolution, one needs much shorter wavelength illumination. Using magnetic lenses, electron microscopy has been applied to the 3D imaging of

thin cellular organelles at a resolution of 3–5 nm (2). The pioneering work on the cryo-electron tomography of cells (2, 79), performed on thin areas in which multiple scattering events are unlikely, has demonstrated clearly the internal complexity and organization of cells. These studies have visualized macromolecular assemblies in the cell around the 5-nm-resolution range. This method of mapping the location of assemblies, however, is limited to samples from either small cells, thin sections of cells, or samples, which can be cryo-sectioned. Even with these restrictions, cryo-electron tomography can visualize large complexes and cytoskeletal architectures in those samples and provide valuable information on their localization.

When comparing light and electron microscopy, one sees a large gap in terms of sample thickness and spatial resolution. X-ray tomography using zone plates for focusing elements can also provide 3D information, currently at ∼60 nm for cells (80), with improvements in optics offering the hope for even higher resolution. This technique also has the disadvantage regarding the defocus across the thickness of the sample, as well as the low efficiency of X-ray usage due to the zone plates. Because of its applicability to thick specimens and its high-resolution imaging capability, X-ray diffraction microscopy is an ideal candidate to bridge the gap between light and electron microscopy and to provide quantitative 3D structural information of whole cells at higher resolution.

With the development of X-ray diffraction microscopes (coupled with high-brightness beam lines with coherence areas greater than the sample size), one can investigate thicker samples—whole eukaryotic or prokaryotic cells and multicellular tissues. Here we illustrate two examples of X-ray diffraction imaging of whole cells. The first is the localization of histidine-tagged proteins inside *Escherichia coli* bacteria (22). The *E. coli* bacteria were transformed with a recombinant protein constructed from a pET-23b vector containing a C-terminal tag with six histidines plus the coding sequence for yellow fluorescent protein; this protein has no bacterial function and was used solely as a marker protein. The yellow fluorescent protein tag enabled visualization in a fluorescence microscope. The bacteria were incubated in a 1% solution of $KMnO_4$ for 10 min, rinsed, applied as a sparse monolayer to a 150-nm-thick silicon nitride substrate, and air dried. $KMnO_4$ acts as a fixative and also reacts to form Mn^{4+} ions that bind to the polyhistidine sequences forming a dense precipitate that strongly diffracts X rays.

Figure 5*a* shows an oversampled diffraction pattern recorded from the manganese-tagged *E. coli* bacteria using 5-keV coherent X rays. The radiation dose to the sample was estimated to be $\sim 8 \times 10^6$ Gy. According to previous experiments (81, 82), this dose would not make any appreciably change in the structure of the sample at this resolution. By using the phase retrieval algorithm, the investigators directly inverted the diffraction pattern to a good-quality image (**Figure 5*b***). Based on the power density spectrum, the resolution was measured to be 30 nm. The reconstructed image is in good agreement with the image obtained from transmission X-ray microscopy (**Figure 5*c***) (83). The slight difference between the two images is likely caused by the different X-ray wavelengths employed and the different imaging mechanisms. The reconstructed image reveals bacteria with a density pattern that bears a remarkable resemblance to the pattern seen from comparable bacteria examined with

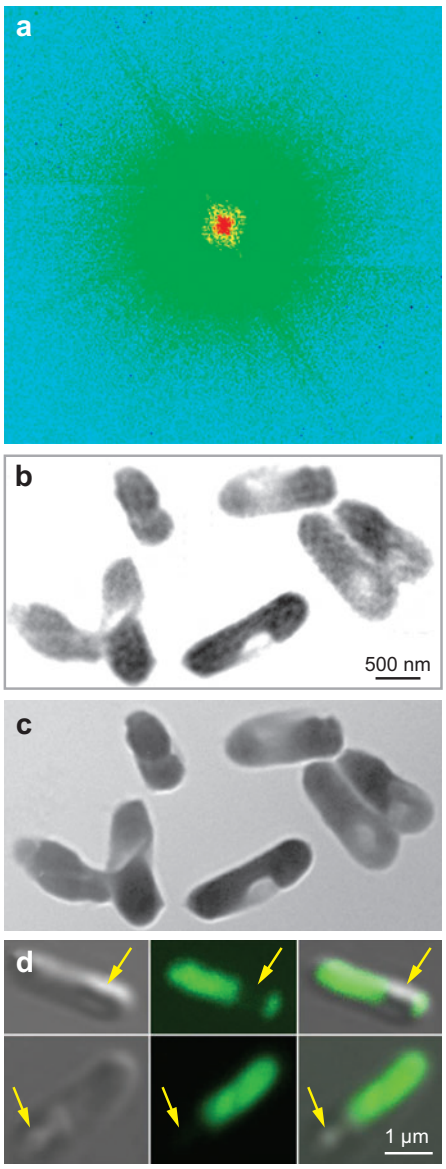

Figure 5

(*a*) Oversampled diffraction pattern from *E. coli* bacteria. (*b*) The corresponding reconstructed image. The dense regions inside the bacteria are likely the distribution of proteins labeled with $KMnO_4$. The semitransparent regions are devoid of yellow fluorescence proteins. (*c*) A transmission X-ray microscopy image of the same specimen. (*d*) Individual bacteria are seen using transmitted light (*left column*) and fluorescence (*middle column*). The yellow fluorescence protein (*green*) is seen throughout most of the bacteria except for one small region in each bacterium that is free of fluorescence (*arrows*). (*Right column*) The fluorescent image superimposed on the transmitted light image. Figure taken from Reference 22.

a confocal microscope (**Figure 5*d***). The fluorescently labeled protein was distributed throughout the entire bacterium, except for one small region in each bacterium that appears devoid of protein (**Figure 5*b***). Similarly, bacteria in the reconstructed image contain dense regions that likely represent the histidine-tagged proteins complexed with manganese and a semitransparent region that is devoid of fluorescent proteins. Although it is not clear what this fluorescent protein-free spot represents, its size and shape are fairly consistent with bacteria seen in both fluorescence and X-ray modalities. Furthermore, the ability to detect this region using fluorescence microscopy on bacteria not yet exposed to X rays precludes the possibility of it being an artifact induced by radiation damage.

The second example is the X-ray diffraction imaging of a yeast, *Saccharomyces cerevisiae* (27, 30). The cells were plunge frozen in liquid ethane and then dried in a commercial freeze dryer. Oversampled diffraction patterns were collected from a single cell using 750-eV X rays. The diffraction pattern was directly inverted to a high-resolution image by the difference map algorithm. Owing to the strong absorption of the cell at this X-ray energy, the reconstructed image is complex valued with the real and imaginary components corresponding to the scattering and absorption, respectively. **Figure 6*a*** shows the complex-valued reconstructed image. By using the power spectrum density, the investigators estimated the resolution of the reconstructed image to be 30 nm. **Figure 6*b*** shows a scanning transmission X-ray microscope image of the same specimen using an X-ray energy of 540 eV (83). Although the two images are in good agreement, the X-ray diffraction microscope image shows a better contrast and a higher resolution than the scanning transmission X-ray microscope image. Furthermore, one can identify some intracellular organelles in **Figure 6*a***, such as a nucleus, a storage vacuole, the cell membrane, and the nuclear membrane.

The reconstructed images shown in **Figure 5*b*** and **Figure 6*a*** represent 2D projections of 3D objects. To identify the 3D intracellular structure and localize specific

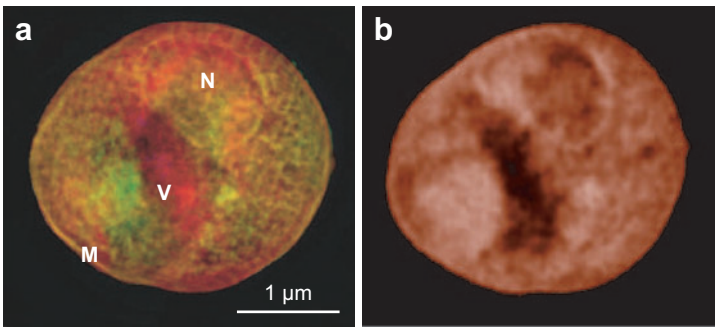

Figure 6

(*a*) X-ray diffraction microscope image of a freeze-dried yeast cell in which N represents a nucleus, V a storage vacuole, and M the cell membrane. (*b*) Scanning transmission X-ray microscope image of the same cell. The brightness represents the magnitude, and the hue represents the phases. Figure taken from Reference 27.

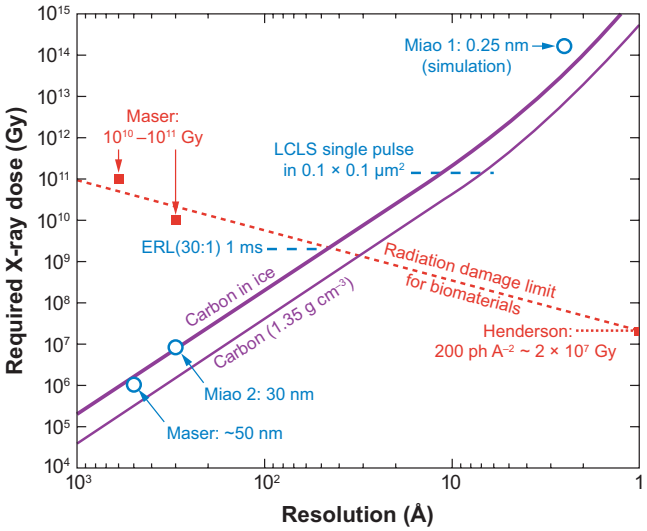

Figure 7

Required X-ray dose at 8 keV to achieve a given spatial resolution for biological samples. A fixed sample volume of $V = 0.1 \times 0.1 \times 0.1\ \mu m^3$ is assumed. Also plotted are several experimental studies from the literature (Henderson refers to Reference 84, Maser to Reference 83, Miao 1 to Reference 99, and Miao 2 to Reference 22). The radiation limit is shown as the dotted red line connecting Henderson's (84) limit at atomic resolution and microscopy studies against mass loss at low resolutions. Figure taken from Reference 85. ERL, Energy Recovery Linac; LCLS, Linac Coherent Light Source.

multiprotein complexes inside whole cells, one needs the 3D image reconstruction of whole cells at a higher resolution. The resolution of X-ray diffraction microscopy is determined by how far the specimen can diffract, which is ultimately limited by radiation damage to the specimen. Several groups have studied the radiation-damage effect in the X-ray diffraction of biological specimens. At atomic resolution, it is commonly accepted that a dose of 2×10^7 Gy would be enough to destroy crystalline orders in protein crystals (84). At lower resolutions, soft X-ray microscopic studies of mass losses in frozen-hydrated cells have shown that a much higher dose of $\sim 10^{10}$ Gy can be tolerated at liquid nitrogen temperatures (81, 82). From the combination of the empirical radiation-damage data and the theoretical estimates on the required dose to achieve a given spatial resolution (**Figure 7**), it has been estimated that the resolution of X-ray diffraction microscopy is likely limited to a few nanometers in three dimensions (85, 86).

Future developments that will be critical to this field are further sample-handling methods, brightness and coherence preserving optics, and detectors with small point-spread function and photon-counting capabilities. The preservation of the samples in their closest-to-native state through the use of frozen-hydrated cells requires significant further advances to make this a routine tool for biologists in their investigation into the biology and architecture of the cell.

OVERCOMING THE RADIATION-DAMAGE BARRIER USING X-RAY FREE ELECTRON LASERS

The Next Generation Source: X-Ray Free Electron Lasers

Although most X-ray diffraction imaging experiments have been carried out with existing synchrotron light sources, scientists need much higher source brightness than is currently available to extend the methods to smaller samples or to achieve higher spatial resolution. An XFEL is a solution to provide the required source brightness.

Madey (87) invented the free electron laser (FEL) in 1971 as a relativistic electron tube using an open optical resonator. In an FEL, a beam of relativistic electrons (produced by an electron accelerator) passes through a transverse, periodic magnetic field (produced by a magnet called an undulator) and exchanges energy with an electromagnetic radiation field in a resonator. The resonance among the electron beam, the undulator field, and the existing electromagnetic radiation field produces an alignment of electrons with a period of a wavelength, which is sometimes referred to as microbunching. The perfectly microbunched electron beam radiates coherently and amplifies the existing radiation. Therefore, the emission rate for the perfectly bunched beam of electrons is proportional to the square of the number of electrons, whereas the emission rate for a beam of randomly positioned electrons is simply proportional to the number of electrons.

The physical principle governing the operation of an FEL is the same in all wavelength regions. However, because there are no X-ray mirrors that are adequate to construct an X-ray resonator, the XFEL was not developed using Madey's original scheme. Instead, all ongoing XFEL plans are based on the self-amplified spontaneous emission process (88, 89). They employ linear accelerators instead of a storage ring as electron accelerators and use sufficiently long undulators as the FEL amplifier. Together with sufficient beam current, the bunching process can be completed in a single pass along the FEL amplifier.

There are three major XFEL construction projects currently in process in the world. The Linac Coherent Light Source, first proposed by Pellegrini (90), is scheduled to operate at the Stanford Linear Accelerator Center in 2009. The Japanese XFEL is scheduled to be complete in 2011, which will be adjacent to the SPring-8 (a third-generation 8-GeV synchrotron light source) at the RIKEN Harima Institute, Japan. In 2013, the European XFEL is scheduled to be complete at the German Electron Synchrotron research center. Each XFEL is expected to have the following properties, which are appropriate for X-ray diffraction microscopy. First, the radiation energy can be easily tuned by changing either the electron-beam energy or magnetic-field strength. Because the lasing medium cannot be damaged by an extremely high optical field, XFELs can produce high peak power exceeding the gigawatt level. Because the temporal pulse structure of the radiation mimics the pulse structure of the electron beam, electron-beam-handling technologies such as the radiofrequency linear accelerator technology can be used to manipulate and control the XFEL pulse structure. Above all, the most remarkable feature is that XFELs easily achieve the desirable properties associated with conventional lasers, such as a

single transverse mode and high spatial and temporal coherence. With these excellent radiation properties, XFELs are regarded as the next generation of X-ray sources.

Overcoming the Radiation-Damage Barrier

Perhaps the most exciting idea proposed in the community to overcome the radiation-damage problem for biological specimens is the use of ultrafast XFEL pulses in coherent diffraction experiments to record a coherent diffraction pattern before the macromolecule explodes in an intense X-ray beam (91, 92). Such proposed XFEL experiments would involve a molecular beam capable of providing a stream of randomly oriented macromolecules, and the recording of a diffraction pattern would be synchronized with the arrival of an X-ray pulse onto a macromolecule in the molecular beam. The incident single-pulse intensity is not strong enough to fully record a high-resolution diffraction pattern, and many thousands of identical copies of each pattern (corresponding to a snapshot of a given molecular orientation) would have to be sorted and added to provide statistically significant signals at the atomic resolution. Theoretical modeling has suggested that in order to make this short-pulse diffraction experiment work, the XFEL pulses need to be shorter than a few femtoseconds (93).

Chapman et al. (31) recently demonstrated experimentally the ultrafast coherent diffraction principle using the FLASH soft X-ray free electron laser in Hamburg, Germany. In that experiment, an intense 25-fs, 4×10^{13} W cm^{-2} pulse, containing 10^{12} photons at 32-nm wavelength, produced a coherent diffraction pattern from a nanostructured nonperiodic object, before destroying it into plasma. A novel X-ray camera assured single-photon detection sensitivity by filtering out parasitic scattering and plasma radiation. The reconstructed image, obtained directly from the coherent pattern by phase retrieval through oversampling, shows no measurable damage, and is reconstructed at a reasonable resolution. This successful experiment indicates that significant damage occurs only after the ultrashort 25-fs FEL pulse traverses the specimen. When shorter-wavelength X-ray lasers become available, more experiments will be necessary to determine how high a resolution flash imaging can be applied.

Other experiments at FLASH on multilayer reflectivity measurements (94) have shown significant reduction in reflectivity during the 25-fs pulse duration at higher pulse intensities. This reduction has been attributed to the modification of the optical constants in the multilayer sample by the irradiation of the intense FLASH laser pulse, not the significant atomic movements or disorders in the multilayer caused by the pulse. These initial results are encouraging and have implications for studying nonperiodic molecular structures in biology, or in any other area of science and technology in which structural information with high spatial and temporal resolution is valuable.

TOWARD IMAGING SINGLE LARGE PROTEIN COMPLEXES

As described in the previous section, theoretical studies have shown that using an extremely bright and ultrashort XFEL pulse, one can collect a 2D diffraction pattern

from a protein molecule before it is destroyed. By using spraying techniques, identical molecules can be selected and injected one by one into an XFEL beam, each generating a 2D diffraction pattern. To assemble a 3D diffraction pattern from these 2D patterns, one needs to determine the orientation of each molecule using one of two methods. The first is to use laser fields to physically align each molecule before the exposure, which has been experimentally demonstrated on small molecules (95). The other is to determine the molecular orientation from the 2D diffraction patterns using the methods developed in cryo-electron microscopy (3, 96). Although either method may result in high noise of the orientation determination, the signal-to-noise ratio can be greatly improved by averaging a large number of molecules at the same orientation and by employing larger protein molecules (e.g., molecular weight >100 kDa) (84). To date, a number of groups have been working on the molecule

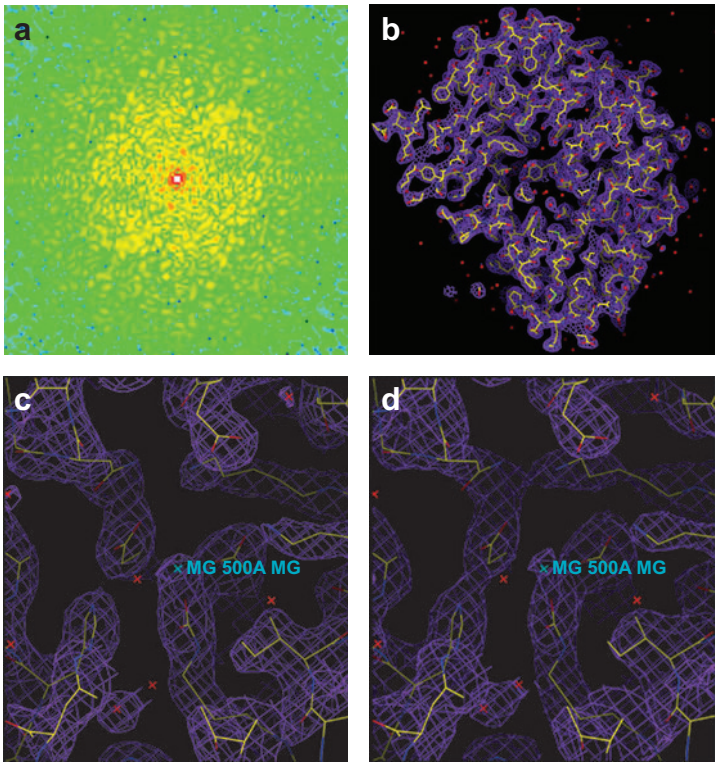

Figure 8

(*a*) One section of a simulated 3D diffraction pattern processed from 10^6 identical copies of the rubisco molecules with Poisson noise added. The edge of the diffraction pattern corresponds to 2.5-Å resolution. The white square at the center corresponds to the missing data owing to a beam stop. (*b*) Stereoview of the 3D electron density map of the rubisco molecule (contoured at two sigma) reconstructed from panel *a* on which the correct atomic model is superimposed. (*c*) The corresponding active site. (*d*) The active site reconstructed from 3×10^5 identical rubisco molecules with Poisson noise added. Figure taken from Reference 97.

injection techniques and the orientation-determination algorithms, obtaining some encouraging results.

After the determination of the molecular orientation, a 3D diffraction pattern can be assembled from the 2D diffraction patterns and then phased to obtain the 3D structure of the molecule. To demonstrate the potential of imaging single large protein molecules using coherent X rays, we give an example on phasing a simulated 3D diffraction pattern from rubisco molecules (97). XFEL pulses were simulated with a wavelength of 1.5 Å, pulse flux of 2×10^{12} photons, a pulse length of 10 fs, and a focal spot of 0.1-μm diameter. Each pulse was synchronized to hit a rubisco molecule and generated a 2D diffraction pattern in which atomic coordinates of the molecule were obtained from the Protein Data Bank. In this simulation, it is assumed that the orientation of each molecule has been determined by the methods described above. By using 10^6 2D diffraction patterns, investigators assembled a 3D diffraction pattern with a size of $160 \times 160 \times 160$ voxels and a resolution of 2.5 Å. To simulate noise, they added Poisson statistical noise to the diffraction pattern. **Figure 8*a*** shows a section of the 3D diffraction pattern. By using the oversampling and iterative phasing algorithm, they reconstructed the 3D electron density of rubisco from the 3D diffraction pattern. **Figure 8*b*,*c*** shows a stereoview of the reconstructed 3D electron density map and the active site, onto which the same atomic model is superimposed. The reconstructed electron density map is almost identical to the true one except for some small differences. To increase the Poisson noise, researchers processed a 3D diffraction pattern from 3×10^5 identical copies of the rubisco molecules and then directly phased it to obtain a 3D electron density map. **Figure 8*d*** shows a stereoview of the reconstructed active site. Compared with **Figure 8*c***, the quality of the reconstructed electron density map deteriorates somewhat as some of the electron density positions in **Figure 8*d*** shift a little bit relative to that in **Figure 8*c***.

SUMMARY POINTS

1. When a diffraction pattern is sampled at a frequency finer than the Nyquist interval so that the oversampling ratio (σ) is larger than 2, the phase information is usually encoded in the diffraction intensity and can be directly recovered using an iterative algorithm.
2. By using the oversampling phasing technique, investigators have successfully extended X-ray crystallography to allow the structural determination of noncrystalline specimens. By avoiding the use of lenses, this methodology is also called lensless imaging (using computation as lenses) or X-ray diffraction microscopy.
3. X-ray diffraction microscopy has been applied to quantitative 3D imaging of noncrystalline materials. The highest resolution achieved thus far is approximately 7 nm, which is mainly limited by the coherent X-ray flux. With

the prospects of more brilliant X-ray sources such as XFELs (68, 69) and energy recovery linacs (98), we anticipate that X-ray diffraction microscopy will be able to image the 3D structure of noncrystalline materials at the near-atomic level.

4. Because X rays have a longer penetration depth than electrons, X-ray diffraction microscopy has been applied to imaging whole *E. coli* and yeast cells at a resolution of 30 nm. By using cryogenic technologies, one should be able to image whole frozen-hydrated cells at a resolution of 10 nm or better in three dimensions, which will allow the localization of specific multiprotein complexes inside the cells.
5. Theoretical studies have shown that, by using extremely intense and ultrashort XFEL pulses, one can record a diffraction pattern from a single biomolecule before it is destroyed. The combination of X-ray diffraction microscopy and XFEL may thus open a new horizon of imaging single large protein molecules without the need of crystallization.
6. The principle of X-ray diffraction microscopy has also been successfully applied to electrons (17, 24) and tabletop high-harmonic soft X-ray sources (99). The tabletop soft X-ray diffraction microscopy is especially attractive for its applications in materials science, nanoscience, and biology.

DISCLOSURE STATEMENT

The authors are not aware of any biases that might be perceived as affecting the objectivity of this review.

ACKNOWLEDGMENTS

We are grateful to our respective collaborators including Changyong Song, Huaidong Jiang, Adrian Mancuso, Chien-Chun Chen, Ting-Kuo Lee, Yoshiki Kohmura, Yoshinori Nishino, Carl Cork, Subhash H. Risbud, Bagrat Amirbekian, and Kevin Raines. This work was supported by the DOE, Office of Basic Energy Sciences (DE-FG02-06ER46276), the NSF (DMR-0520894), and RIKEN, Japan.

LITERATURE CITED

1. Rule GS, Hitchens TK. 2006. *Fundamentals of Protein NMR Spectroscopy*. Dordrecht: Springer
2. Medalia O, Weber I, Frangakis AS, Nicastro D, Gerisch G, Baumeister W. 2002. Macromolecular architecture in eukaryotic cells visualized by cryoelectron tomography. *Science* 298:1209–13
3. Frank J. 2002. Single-particle imaging of macromolecules by cryo-electron microscopy. *Annu. Rev. Biophys. Biomol. Struct.* 31:303–19

4. Miao J, Chapman HN, Kirz J, Sayre D, Hodgson KO. 2004. Taking X-ray diffraction to the limit: macromolecular structures from femtosecond X-ray pulses and diffraction microscopy of cells with synchrotron radiation. *Annu. Rev. Biophys. Biomol. Struct.* 33:157–76
5. Robinson IK, Miao J. 2004. Three-dimensional coherent X-ray diffraction microscopy. *MRS Bull.* 29:177–81
6. Miao J, Kirz J, Sayre D. 2000. The oversampling phasing method. *Acta Cryst.* 56:D1312–15
7. Miao J, Sayre D, Chapman HN. 1998. Phase retrieval from the magnitude of the Fourier transforms of nonperiodic objects. *J. Opt. Soc. Am. A* 15:1662–69
8. Fienup JR. 1978. Reconstruction of an object from the modulus of its Fourier transform. *Opt. Lett.* 3:27–29
9. Miao J, Sayre D. 2000. On possible extensions of X-ray crystallography through diffraction-pattern oversampling. *Acta Cryst.* 56:A596–605
10. Elser V. 2003. Phase retrieval by iterated projections. *J. Opt. Soc. Am. A* 20:40–55
11. Marchesini S. 2007. A unified evaluation of iterative projection algorithms for phase retrieval. *Rev. Sci. Instrum.* 78:011301
12. Sayre D. 1980. Prospects for longwavelength X-ray microscopy and diffraction. In *Imaging Processes and Coherence in Physics*, ed. M Schlenker, M Fink, JP Goedgebuer, C Malgrange, JC Vienot, RH Wade, pp. 229–35. Vol. 112, Springer Lect. Notes Phys. Berlin: Springer
13. Sayre D. 1991. Note on "superlarge" structures and their phase problem. In *Direct Methods of Solving Crystal Structures*, ed. H Schenck, pp. 353–56. New York: Plenum
14. **Miao J, Charalambous P, Kirz J, Sayre D. 1999. Extending the methodology of X-ray crystallography to allow imaging of micrometer-sized noncrystalline specimens. *Nature* 400:342–44**
15. Robinson IK, Vartanyants IA, Williams GJ, Pferfer MA, Pitney JA. 2001. Reconstruction of the shapes of gold nanocrystals using coherent X-ray diffraction. *Phys. Rev. Lett.* 87:195505
16. **Miao J, Ishikawa T, Johnson B, Anderson EH, Lai B, Hodgson KO. 2002. High resolution 3D X-ray diffraction microscopy. *Phys. Rev. Lett.* 89:088303**
17. Miao J, Ohsuna T, Terasaki O, Hodgson KO, O'Keefe MA. 2002. Atomic resolution three-dimensional electron diffraction microscopy. *Phys. Rev. Lett.* 89:155502
18. Nishino Y, Miao J, Ishikawa T. 2003. Image reconstruction of nanostructured nonperiodic objects only from oversampled hard X-ray diffraction intensities. *Phys. Rev. B* 68:220101
19. Miao J, Amonette JE, Nishino Y, Ishikawa T, Hodgson KO. 2003. Direct determination of the absolute electron density of nanostructured and disordered materials at sub-10-nm resolution. *Phys. Rev. B* 68:012201
20. Marchesini S, He H, Chapman NH, Hau-Riege SP, Noy A, et al. 2003. X-ray image reconstruction from a diffraction pattern alone. *Phys Rev. B* 68:140101
21. **Nugent KA, Peele AG, Chapman HN, Mancuso AP. 2003. Unique phase recovery for nonperiodic objects. *Phys. Rev. Lett.* 91:203902**

14. First experimental demonstration of extending X-ray crystallography to the imaging of noncrystalline specimens.

16. Reports the first experimental demonstration of 3D X-ray diffraction microscopy.

21. Proposes a method to uniquely retrieve the phases from oversampled diffraction patterns by using X-ray fields with phase curvature.

22. Miao J, Hodgson KO, Ishikawa T, Larabell CA, LeGros MA, Nishino Y. 2003. Imaging whole *Escherichia coli* bacteria by using single-particle X-ray diffraction. *Proc. Natl. Acad. Sci. USA* 100:110–12

23. Williams GJ, Pfeifer MA, Vartanyants IA, Robinson IK. 2003. Three-dimensional imaging of microstructure in Au nanocrystals. *Phys. Rev. Lett.* 90: 175501

24. Zuo JM, Vartanyants I, Gao M, Zhang R, Nagahara LA. 2003. Atomic resolution imaging of a carbon nanotube from diffraction intensities. *Science* 300:1419–21

25. Eisebitt S, Lorgen M, Eberhardt W, Luning J, Andrews S, Stohr J. 2004. Scalable approach for lensless imaging at X-ray wavelengths. *App. Phys. Lett.* 84:3373–75

26. Xiao X, Shen Q. 2005. Wave propagation and phase retrieval in Fresnel diffraction by a distorted-object approach. *Phys. Rev. B* 72:033103

27. Shapiro D, Thibault P, Beetz T, Elser V, Howells M, et al. 2005. Biological imaging by soft X-ray diffraction microscopy. *Proc. Natl. Acad. Sci. USA* 102:15343–46

28. Miao J, Nishino Y, Kohmura Y, Johnson B, Song CY, et al. 2005. Quantitative image reconstruction of GaN quantum dots from oversampled diffraction intensities alone. *Phys. Rev. Lett.* 95:085503

29. Quiney HM, Peele AG, Cai Z, Paterson D, Nugent KA. 2006. Diffractive imaging of highly focused X-ray fields. *Nat. Phys.* 2:101–4

30. Thibault P, Elser V, Jacobsen C, Shapiro D, Sayre D. 2006. Reconstruction of a yeast cell from X-ray diffraction data. *Acta Cryst. A* 62:248–61

31. Chapman HN, Barty A, Bogan MJ, Boutet S, Frank M, et al. 2006. Femtosecond diffractive imaging with a soft X-ray free electron laser. *Nat. Phys.* 2:839–44

32. Pfeifer MA, Williams GJ, Vartanyants IA, Harder R, Robinson IK. 2006. Three-dimensional mapping of a deformation field inside a nanocrystal. *Nature* 442:63–66

33. Williams GJ, Quiney HM, Dhal BB, Tran CQ, Nugent KA, et al. 2006. Fresnel coherent diffractive imaging. *Phys. Rev. Lett.* 97:025506

34. Chapman HN, Barty A, Marchesini S, Noy A, Hau-Riege SP, et al. 2006. High resolution ab initio three-dimensional X-ray diffraction microscopy. *J. Opt. Soc. Am. A* 23:1179–200

35. Miao J, Chen CC, Song C, Nishino Y, Kohmura Y, et al. 2006. Coherent X-ray diffraction microscopy reveals three-dimensional GaN-Ga_2O_3 core shell structures at the nanometer scale. *Phys. Rev. Lett.* 97:215503

36. Gaffney KJ, Chapman HN. 2007. Imaging atomic structure and dynamics with ultrafast X-ray scattering. *Science* 316:1444–48

37. Rodenburg JM, Hurst AC, Cullis AG, Dobson BR, Pfeiffer F, et al. 2007. Hard-X-ray lensless imaging of extended objects. *Phys. Rev. Lett.* 98:034801

38. Song C, Ramunno-Johnson D, Nishino Y, Kohmura Y, Ishikawa T, et al. 2007. Phase retrieval from exactly oversampled diffraction intensity through deconvolution. *Phys. Rev. B* 75:012102

22. Describes the first experiment recording and reconstruction of the diffraction pattern from a biological specimen (i.e., *E. coli* bacteria) at 30-nm resolution using coherent X rays.

27. Uses X-ray diffraction microscopy to image the complex valued exit wave of an intact and unstained yeast cell and proposes a technique to determine the reconstructed resolution.

31. First experimental demonstration that the diffraction pattern of a noncrystalline specimen can be recorded before it is destroyed by a soft XFEL pulse.

32. Reports a novel experiment of revealing the 3D evolution of a deformation field inside a lead nanocrystal by inverting the coherent X-ray diffraction pattern.

37. Reports a novel X-ray diffraction imaging experiment for extended objects, based on the combination of ptychography with an iterative phase-retrieval algorithm.

39. Takahashi Y, Nishino Y, Ishikawa T, Matsubara E. 2007. Approach for three-dimensional observation of mesoscopic precipitates in alloys by coherent X-ray diffraction microscopy. *Appl. Phys. Lett.* 90:184105
40. European Synchrotron Radiation Facility. *International workshop on phase retrieval and coherent scattering*. **http://www.esrf.eu/events/conferences/past-conferences-and-workshops/Coherence2005/**
41. Shen Q, Hao Q, Gruner SM. 2006. Macromolecular phasing. *Phys. Today* 59:46–52
42. Nugent KA, Paganin D, Gureyev TE. 2001. A phase odyssey. *Phys. Today* 54:27–32
43. Patterson AL. 1934. A Fourier series method for the determination of the components of interatomic distances in crystals. *Phys. Rev. B* 46:372–76
44. Giacovazzo C. 1998. *Direct Phasing in Crystallography*. New York: Oxford Univ. Press
45. Green DW, Ingram VM, Perutz MF. 1954. The structure of haemolglobin. IV. Sign determination by the isomorphous replacement method. *Proc. R. Soc. Lond. Ser. A* 255:287–307
46. Argos P, Rossman MG. 1980. Molecular replacement method. In *Theory and Practice of Direct Methods in Crystallography*, ed. MFC Ladd, RA Palmer, pp. 361–417. New York: Plenum
47. Phillips JC, Wlodawer A, Goodfellow JM, Watenpaugh KD, Sieker LC, et al. 1977. Applications of synchrotron radiation to protein crystallography. II. Anomalous scattering, absolute intensity, and polarization. *Acta Cryst.* 33:A445–55
48. Hendrickson WA, Smith JL, Sheriff S. 1985. Direct phase determination based on anomalous scattering. *Methods Enzymol.* 115:41–55
49. Wang BC. 1985. Resolution of phase ambiguity in macromolecular crystallography. *Methods Enzymol.* 115:90–112
50. Bricogne G. 1974. Geometric sources of redundancy in intensity data and their use for phase determination. *Acta Crystallogr.* 30:A395–405
51. Rossmann MG, Blow DM. 1963. Determination of phases by the conditions of noncrystallographic symmetry. *Acta Crystallogr.* 16:39–45
52. Hao Q. 2001. Phasing from an envelope. *Acta Cryst.* 57:D1410–14
53. Weckert E, Hummer K. 1997. Multiple-beam X-ray diffraction for physical determination of reflection phases and its applications. *Acta Cryst.* 53:A108–43
54. Shen Q, Wang J. 2003. Recursive direct phasing with reference-beam diffraction. *Acta Cryst.* 59:D809–14
55. Shannon CE. 1949. Communication in the presence of noise. *Proc. IRE* 37:10–21
56. Bates RHT. 1982. Fourier phase problem are uniquely soluble in more than one dimension. I: Underlying theory. *Optik* 61:247–62
57. Blankenbecler R. 2004. Three-dimensional image reconstruction. II. Hamiltonian method for phase recovery. *Phys. Rev. B* 69:064108
58. Gerchberg RW, Saxton WO. 1972. A practical algorithm for the determination of phase from image and diffraction plane pictures. *Optik* 35:237–46

59. Chen CC, Miao J, Wang CW, Lee TK. 2007. Application of the optimization technique to noncrystalline X-ray diffraction microscopy: guided hybrid input-output method (GHIO). *Phys. Rev. B* 76:064113
60. Aoki S, Kagoshima Y, Suzuki Y, eds. 2006. *X-Ray Microscopy. Proc. 8th Int. Conf.* IPAP Conf. Ser. 7. Tokyo: Inst. Pure Appl. Phys.
61. Chao W, Harteneck BD, Liddle JA, Anderson EH, Attwood DT. 2005. Soft X-ray microscopy at a spatial resolution better than 15 nm. *Nature* 435:1210–13
62. Jacobsen C, Kirz J, Williams S. 1992. Resolution in soft X-ray microscopes. *Ultramicroscopy* 47:55–79
63. Jiang H, Ramunno-Johnson D, Song C, Amirbekian B, Kohmura Y, et al. 2007. Nanoscale imaging of mineral crystals inside biological composite materials using X-ray diffraction microscopy. *Phys. Rev. Lett.* In press
64. Tong J, Risbud SH. 2004. Processing and structure of gallium nitride: gallium oxide platelet nanostructures. *J. Solid State Chem.* 177:3568–74
65. Spence JCH. 2003. *High-Resolution Electron Microscopy*. New York: Oxford Univ. Press. 3rd ed.
66. Meyer E, Jarvis SP, Spencer ND. 2004. Scanning probe microscopy in materials science. *MRS Bull.* 29:443–48
67. Miao J, Ishikawa T, Anderson EH, Hodgson KO. 2003. Phase retrieval of diffraction patterns from noncrystalline samples. *Phys. Rev. B* 67:174104
68. S'Shea PG, Freund HP. 2001. Free-electron lasers: status and applications. *Science* 292:1853–58
69. Pellegrini C, Stohr J. 2003. X-ray free-electron lasers: principles, properties and applications. *Nucl. Instrum. Methods A* 500:33–40
70. Sali A, Glaeser R, Earnest T, Baumeister W. 2003. From words to literature in structural proteomics. *Nature* 422:216–25
71. Chandonia JM, Earnest TN, Brenner S. 2004. Structural genomics and structural biology: compare and contrast. *Genome Biol.* 5:343–47
72. Cheyette BNR, Waxman JS, Miller JR, Takemaru K-I, Sheldahl LC, et al. 2002. Dapper, a Dishevelled-associated antagonist of ß-catenin and JNK signaling, is required for notochord formation. *Dev. Cell* 2:449–61
73. Krogan NJ, Cagney G, Yu H, Zhong G, Guo X, et al. 2006. Global landscape of protein complexes in the yeast *Saccharomyces cerevisiae*. *Nature* 440:637–43
74. Shapiro L, McAdams HH, Losick R. 2002. Generating and exploiting polarity in bacteria. *Science* 298:1942–46
75. Gitai Z. 2005. The new bacterial cell biology: moving parts and subcellular architecture. *Cell* 120:577–86
76. Hurtley SM, Helmuth L, eds. 2003. Special issue on biological imaging. *Science* 300:75–100
77. Willig KI, Rizzoli S, Westphal V, Jahn R, Hell SW. 2006. STED microscopy reveals that synaptotagmin remains clustered after synaptic vesicle exocytosis. *Nature* 440:935–39
78. Betzig E, Patterson GH, Sougrat R, Lindwasser OW, Olenych S, et al. 2006. Imaging intracellular fluorescent proteins at nanometer resolution. *Science* 313:1642–45

79. McIntosh R, Nicastro D, Mastronarde DN. 2005. New views of cells in 3D: an introduction to electron tomography. *Trends Cell Biol.* 15:43–51
80. Le Gros MA, McDermott G, Larabell CA. 2005. X-ray tomography of whole cells. *Curr. Opin. Struct. Biol.* 15:593–600
81. Maser J, Osanna A, Wang S, Jacobsen C, Kirz J, et al. 2000. Soft X-ray microscopy with a cryo STXM: I. Instrumentation, imaging, and spectroscopy. *J. Microsc.* 197:68–79
82. Schneider G. 1998. Cryo X-ray microscopy with high spatial resolution in amplitude and phase contrast. *Ultramicroscopy* 75:85–104
83. Kirz J, Jacobsen C, Howells M. 1995. Soft X-ray microscopes and their biological applications. *Q. Rev. Biophys.* 28:33–130
84. Henderson R. 1995. The potential and limitations for neutrons, electrons and X rays for atomic resolution microscopy of unstained biological molecules. *Q. Rev. Biophys.* 28:171–93
85. Shen Q, Bazarov I, Thibault P. 2004. Diffractive imaging of nonperiodic materials with future coherent X-ray sources. *J. Synchrotron Rad.* 11:432–38
86. Howells MR, Beetz T, Chapman HN, Cui C, Holton JM, et al. 2007. An assessment of the resolution limitation due to radiation damage in X-ray diffraction microscopy. *J. Electron. Spectrosc. Rel. Phenom.* In press
87. Madey JM. 1971. Stimulated emission of bremsstrahlung in a periodic magnetic field. *J. Appl. Phys.* 42:1906–13
88. Bonifacio R, Pellegrini C, Narducci LM. 1985. Collective instabilities and high gain regime in a free-electron lasers. *Opt. Commun.* 50:373–78
89. Kim KJ. 1986. Three-dimensional analysis of coherent amplification and self-amplified spontaneous emission in free electron lasers. *Phys. Rev. Lett.* 57:1871–74
90. Pellegrini C. 1992. A 4 to 0.1 FEL based on the SLAC Linac. *Proc. Workshop 4th Gener. Light Sources*, ed. M Cornacchia, H Winick, pp. 376–84. Stanford, CA: SLAC
91. Neutze R, Wouts R, Spoel D, Weckert E, Hajdu J. 2000. Potential for biomolecular imaging with femtosecond X-ray pulses. *Nature* 406:752–57
92. Hajdu J. 2000. Single-molecule X-ray diffraction. *Curr. Opin. Struct. Biol.* 10:569–73
93. Hau-Riege SP, London RA, Szoke A. 2004. Dynamics of biological molecules irradiated by short X-ray pulses. *Phys. Rev. E* 69:51906
94. Hau-Riege SP, Chapman HN, Krzywinski J, Sobierajski R, Bajt S, et al. 2007. Subnanometer-scale measurements of the interaction of ultrafast soft X-ray free-electron-laser pulses with matter. *Phys. Rev. Lett.* 98:145502
95. Larsen JJ, Hald K, Bjerre N, Stapelfeldt H, Seideman T. 2000. Three-dimensional alignment of molecules using elliptically polarized laser fields. *Phys. Rev. Lett.* 85:2470–73
96. Crowther RA. 1971. Procedures for three-dimensional reconstruction of spherical viruses by Fourier synthesis from electron micrographs. *Philos. Trans. R. Soc. Lond. Ser. B* 261:221–30
97. Miao J, Hodgson KO, Sayre D. 2001. An approach to three-dimensional structures of biomolecules by using single-molecule diffraction images. *Proc. Natl. Acad. Sci. USA* 98:6641–45

91. Using computer simulations, shows that biomolecules can withstand an X-ray intensity of $\sim 3.8 \times 10^6$ photons $Å^{-2}$ within approximately 10 fs with minimal structural changes.

97. Proposes a new approach to the high-resolution 3D structural determination of macromolecules that utilizes ultrashort, intense X-ray pulses and the oversampling phasing method.

98. Bilderback DH, Bazarov IV, Finkelstein K, Gruner SM, Padamsee HS, et al. 2003. Energy-recovery linac project at Cornell University. *J. Synchrotron Rad.* 10:346–48
99. Sandberg RL, Paul A, Raymondson D, Hädrich S, Gaudiosi D, et al. 2007. Lensless diffractive imaging using tabletop, coherent, high harmonic soft X-ray beams. *Phys. Rev. Lett.* 99:098103